Mapping Band Alignment across Complex Oxide Heterointerfaces

Bo-Chao Huang,[1] Ya-Ping Chiu,[1,*] Po-Cheng Huang,[1] Wen-Ching Wang,[1] Vu Thanh Tra,[2] Jan-Chi Yang,[3] Qing He,[4] Jiunn-Yuan Lin,[2] Chia-Seng Chang,[5] and Ying-Hao Chu[3]

[1]*Department of Physics, National Sun Yat-sen University, Kaohsiung 804, Taiwan*
[2]*Institute of Physics, National Chiao Tung University, Hsinchu 300, Taiwan*
[3]*Department of Materials Science and Engineering, National Chiao Tung University, HsinChu 300, Taiwan*
[4]*Advanced Light Source, Lawrence Berkeley National Laboratory, Berkeley, California 94720, USA*
[5]*Institute of Physics, Academia Sinica, Taipei 105, Taiwan*

(Received 15 March 2012; published 12 December 2012)

In this study, direct observation of the evolution of electronic structures across complex oxide interfaces has been revealed in the $LaAlO_3/SrTiO_3$ model system using cross-sectional scanning tunneling microscopy and spectroscopy. The conduction and valence band structures across the $LaAlO_3/SrTiO_3$ interface are spatially resolved at the atomic level by measuring the local density of states. This study directly maps out the electronic reconstructions and a built-in electric field in the polar $LaAlO_3$ layer. Results also clearly reveal the band bending and the notched band structure in the $SrTiO_3$ adjacent to the interface.

DOI: 10.1103/PhysRevLett.109.246807 PACS numbers: 73.20.−r, 68.35.−p, 68.37.−d

Interfaces have emerged as a key focal point in current condensed matter science. In complex correlated oxides, heterointerfaces provide a powerful way to design and manipulate the charge, spin, orbital, and lattice degrees of freedom [1]. In artificially constructed heterointerfaces, the interactions between these degrees of freedom have led to a number of exciting discoveries [2–6]. Cross-sectional scanning tunneling microscopy and spectroscopy (XSTM/S) have recently been applied to explore the electronic structures across domain walls in ferroics with atomic resolution [7]. These approaches provide direct experimental insights into the origin and nature of electrical conductivity at these homointerfaces. The present study probes the electronic structures across the heterointerfaces between different materials in complex oxides using this technique. These heterostructured systems are challenging because the different band structures of the materials on both sides of the interface and extrinsic effects, such as tip-sample interactions, must be taken into account [8,9].

The conducting quasi-two-dimensional electron gas formed at the interface between two insulators [$LaAlO_3$ (LAO) and $SrTiO_3$ (STO)] is an intriguing example [2]. Researchers have proposed possible scenarios to explain the metallic behavior at the LAO/STO interface and conceptually defined them with interfacial band diagrams across the heterojunction [10–17]. Although several studies have investigated the electronic structure of the LAO/STO interface both experimentally and theoretically [3,13,16–18], technologies capable of addressing the nature of the interfacial charge of LAO/STO *locally* and *directly* in real space remain to be developed. Therefore, the need to directly determine the electronic configuration between LAO and STO as well as interfacial electrostatic boundary conditions form the motivation for this study.

To address this issue, the LaO^+-TiO_2 interface was fabricated using pulsed laser deposition assisted with reflection high-energy electron diffraction. To prevent tip crash in STM measurements, the experiments used 0.5 wt.% Nb doped STO substrates (Nb-STO). An atomically smooth surface with clear unit cell (u.c.)-height steps on the TiO_2-terminated Nb-STO substrate was observed with atomic force microscopy before the thin film depositions. To inhibit the influence of the doped substrates, an STO layer (10 u.c.) was deposited prior to the growth of LAO layers. Then, a 5-u.c. LAO thin film was grown on the TiO_2-terminated STO to investigate the band structure of the LAO/STO system. The films were grown at 850 °C under an oxygen pressure of 2×10^{-5} Torr. After the growth of the LAO layer, we cooled the samples to 700 °C at 1 Torr in the chamber and injected oxygen close to 500 Torr for 20 min, and then cooled the samples to room temperature. The thickness of films was controlled atomically by monitoring the intensity oscillation of the specular spot in reflection high-energy electron diffraction. Transport measurements were performed to confirm the metallic behavior of this interface. When the transport measurements performed on the 10-u.c. STO/Nb-STO samples before the growth of LAO, these surfaces did not appear as conductive. However, the critical LAO thickness of 4 u.c. for the onset of interfacial conductivity is detected. Finally, an amorphous $SrRuO_3$ (SRO) buffer layer (500 nm) was then deposited on the LAO at room temperature to prevent tip crash in STM measurements. The SRO/5-u.c.–LAO/STO/Nb-STO sample was then cleaved *in situ* at room temperature in an ultrahigh vacuum chamber with a base pressure of approximately 5×10^{-11} Torr and all STM measurements were performed at ~60 K and taken from the cross-sectional view

[Fig. 1(a)] [19,20]. Figure 1(b) shows a cross-sectional constant current STM image of the LAO/STO heterostructure with a sample bias of −3.0 V. The apparent height contrast is mainly originated from the spectroscopic effect attributable to the significant discrepancy of the local density of states in this heterostructured system at the −3.0 V sample bias. With reference to the growth sequence, the thickness of the layers, and the changes in the electronically specific tunneling spectra between SRO and Nb-STO as the probe moves across the heterostructure, this makes it practical to accurately locate each layer and examine the interfacial electronic structures across the LAO/STO interface. With the addition of scanning tunneling spectroscopy (STS) measurements at approximately 60 K, it is possible to obtain direct information on the local electronic structures at the LAO/STO heterointerface.

This study clearly demonstrates the direct imaging of unusual electronic properties at the interface of the LAO/STO heterojunction region from the cross section using STS measurements. Figure 1(c) shows a local density of states (LDOS) image taken at +1.0 V at the interface of the LAO/STO heterojunction. This figure clearly shows a dramatic electronic structure change at the interface [indicated by the red arrow in Fig. 1(c)], displaying the unique variation of electronic properties on the STO side of the interface. Basically, at positive sample bias, the increase of the tunneling current signal corresponds to a substantial increase in the number of local filled states above the Fermi level (E_F) at the interface. Therefore, the unusual electronic properties at the interface of the STO side may originate from the band bending and the accumulation of surface charges in the STO adjacent to the interface.

Scanning tunneling spectroscopy is a powerful tool for resolving spatial variations of the local electronic structures near E_F with high resolution. Therefore, efforts have been made to utilize it to acquire and collect spatially resolved tunneling spectra at spatial locations on either side of the interface. Meanwhile, using the first derivative of tunneling current over tip-sample voltage or differential conductivity, dI/dV, a measurement of the LDOS was performed using STS [21,22]. Figure 2 shows spatially resolved spectroscopic measurements through the 5-u.c. LAO/STO heterointerface. The colored solid bars in the current image [Fig. 2(a)] mark the spatial positions across the interface, and Fig. 2(b) shows the corresponding tunneling spectra [21–23]. The colored brown spectra belong to the spectroscopic results of the thin $SrTiO_3$ film from the position away from the STO/LAO interface [spectrum i in Fig. 2(b)], and the red spectrum indicates the result of the $SrTiO_3$ film adjacent to the interface [spectrum ii in Fig. 2(b)]. The colored blue spectrum represents the spectroscopic results of the thin 5-u.c. $LaAlO_3$ film from the position near the STO/LAO interface [spectrum iii in Fig. 2(b)] to that away from the interface [spectrum iv in Fig. 2(b)]. This study uses the methodology previously

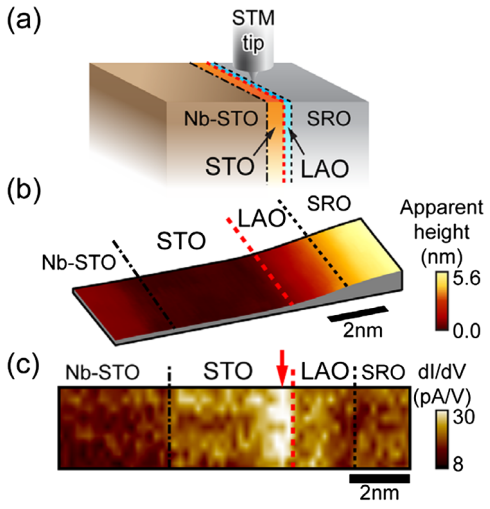

FIG. 1 (color online). (a) Cross-sectional STM/S is employed to investigate the properties at the interface. (b) A typical cross-sectional constant current STM image of the epitaxial LAO/STO heterostructure obtained at a sample bias of −3.0 V. (c) The spectroscopic measurements of LAO/STO interface at +1.0 V sample bias. The unusual electronic property at the interface is specifically shown by the red arrow. The dashed red lines are indicated as the interface of LAO/STO.

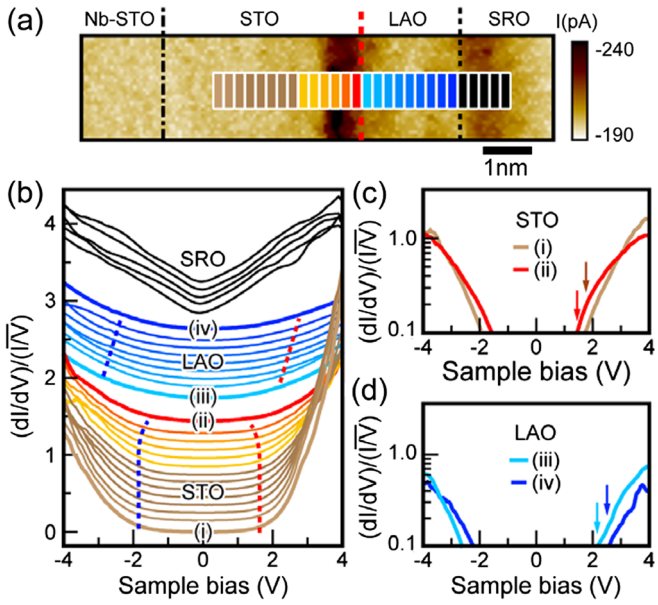

FIG. 2 (color online). (a) Current image of LAO/STO obtained at −3 V sample bias. Under the condition, the current image reasonably reflects the drastic discrepancy attributable to the electronic property at the heterointerfaces. (b) The corresponding atomic-scale evolution of electronic properties across the heterointerfaces of 5-u.c. LAO/STO. (c) The determination of band edges of STO side away (spectrum i) and near (spectrum ii) the interface of LAO/STO. (d) The determination of band edges of LAO side near (spectrum iii) and away (spectrum iv) from the interface of LAO/STO.

applied in Ref. [21] to determine the onset energies for band extreme based on the assumption of a linear region on either side of the onset in normalized conductance. The precision of the onset energies determined by this method is approximately ± 0.10 eV in this study. Based on normalized dI/dV curves, the dashed red and blue lines in Fig. 2(b) represent the onsets of the tunneling current in empty and filled states, respectively.

When analyzing spectrum i and spectrum ii extracted from STO in Fig. 2(b), the current onsets are estimated to be $+1.70$ V/-1.75 V in spectrum i and $+1.45$ V/-1.55 V in spectrum ii, respectively [Fig. 2(c)]. These results clearly demonstrate the energy shift of the band onset in the STO adjacent to the interface of 5-u.c. LAO/STO. In addition, the determination of the current onsets on the LAO side near and away from the interface can also be applied using the same analysis methodology performed to STO. When analyzing the spectrum iii (near interface) and spectrum iv (away from the interface) extracted from Fig. 2(b) in LAO, the current onsets are estimated to be $+2.30$ V/-2.90 V in spectrum iii and $+2.90/-2.30$ V in spectrum iv, respectively [Fig. 2(d)]. Using the extracted potential difference between spectra iii and iv [Fig. 2(d)], the magnitude of the built-in electric field in LAO can be calculated to be (30 ± 5) meV Å^{-1} for 5-u.c. LAO.

Based on the characteristics of the spatial spectroscopic measurements in Figs. 2(b) and 3 quantitatively constructs and maps the evolution of band alignment across the heterointerface. The features of the band alignment of the heterostructure, the notched structure in the STO adjacent to the interface, are observed. Furthermore, the charge carrier accumulation at the band notches (ΔV) at the STO side of the interface to an approximate distance (λ) of 0.8 nm is directly revealed. In addition, the features of the band alignment between adjacent LAO atomic layers

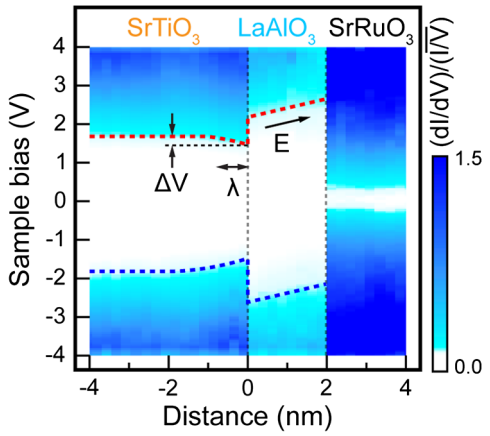

FIG. 3 (color online). Experimentally measured band alignment of 5-u.c. LAO/STO. The analysis is to normalize the differential conductance (dI/dV) to ($\overline{I/V}$), the general total conductance background [21,22].

also confirm the existence of a built-in electric field (E) in the LAO layer, which is partially compensated by the electron gas or covalency within the thin film [12,13].

Attempts to provide quantitative descriptions of tunneling spectra from samples and schematically map the band alignment across complex oxide heterointerfaces are also made in the work. A significant consideration to the quantitative description of tunneling spectra from samples is the occurrence of the tip-induced band bending in the system [24–27]. When a sharp probe tip is close to a semiconductor or oxide surface, the resulting electrostatic potential distributions bring forth some of the applied potential between tip and sample being dropped in the sample itself. The effect of the varying electrostatic potential in the semiconductor is to shift the energy bands. The potential distribution and the resulting shift of the energy bands can thus play an important role in determining the measured signal. Therefore, in this work, to present a solution for the electrostatic problem of a probe tip near a surface, previous research has developed a three-dimensional (3D) potential computation technique for solving the electrostatic problem of a probe tip near a semiconductor [25–27]. With the electrostatic potential computed in a fully 3D model, a full numerical integration can be performed in computing the current. Using the theoretical considerations, we are able to realize the physical situation when the tip approximates the surface during STM measurements, numerically fit experimental spectra, and evaluate the tip-induced band bending (TIBB) effect [24]. In this 3D computation model, the value of 0.53 eV is given by the difference between the work function of the tungsten (W) tip and the STO electron affinity [28,29]. The dielectric constants of STO and LAO are 180 and 25, respectively [30,31]. Within effective mass approximation, there is fairly good agreement between the simulated and measured tunneling spectra of the STO surface when the distance between the tip and the sample (d) is 0.3 nm. The theoretical modeling can realize the variation of the surface potential as a function of the sample bias and extract the energetic positions of the conduction band and valence band (CB and VB) edges of the system [24]. Figures 4(a)–4(c) illustrate the schematic band level diagrams of the sample and the tip during STM measurements. In Fig. 4(a), the band structure models the situation when the measurement is performed on the STO surface away from the interface (simulated the experimental spectrum i situation). The simulation result in Fig. 4(a) suggests that the energetic CB and VB band edges of the STO region away from the interface are $+1.30$ V/-1.90 V on the surface and $+0.28$ V/-2.92 V in bulk at the zero sample bias. In addition, when the measurement is performed on the STO surface at the interface (simulated the experimental spectrum ii situation), at the zero sample bias, the band edges of the STO region at the interface are $+1.22$ V/-1.98 V on the surface and suggested -0.03 V/-3.23 V in bulk [Fig. 4(b)]. The result

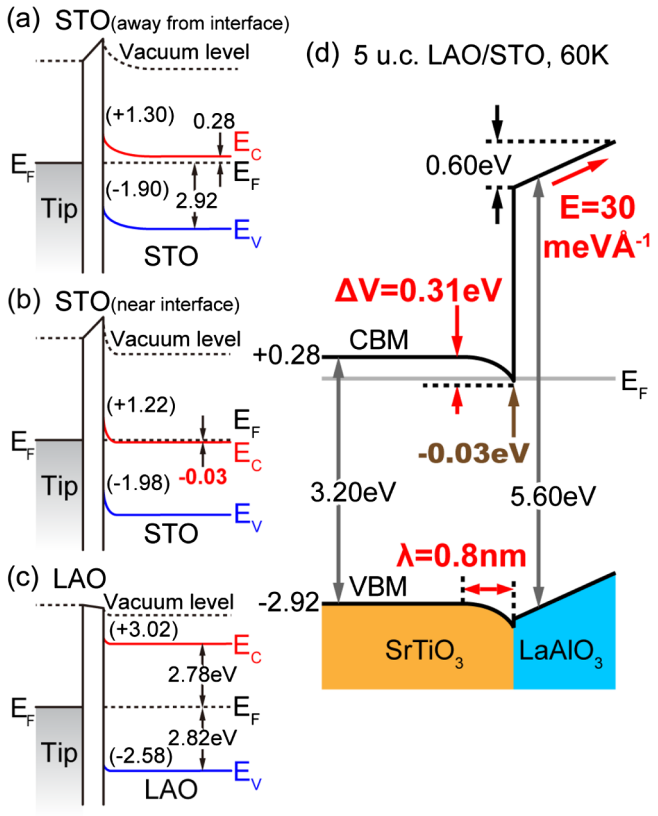

FIG. 4 (color online). According to the self-consistent solutions for the present heterostructured system, theoretical calculations on the band edges of the STO region located (a) away from interface, and (b) at the interface at the zero sample bias. (c) Theoretical calculations on the band edges of the LAO region neutrally centered at the middle of the film at zero sample bias. (d) A schematic band alignment of the 5-u.c. LAO/STO heterointerfaces.

indicates that the CB edge in STO at the interface is located below E_F (-0.03 V) and elucidates the formation of two-dimensional electron confinement at the LAO/STO heterointerfaces. Furthermore, the same simulation and analysis methodology was also applied to the LAO. The schematic band structure in Fig. 4(c) indicates the energetic CB and VB edges of LAO at the neutral potential situation are $+2.78$ V and -2.82 V in bulk.

Through a rigorous calibration procedure based on considerations of the TIBB effect, Fig. 4(d) shows the schematic band alignments of metallic LAO/STO interfaces with 5-u.c. LAO thicknesses. The interfacial band diagram in Fig. 4(d) demonstrates the interfacial electronic characteristics of the STO/LAO heterostructure [32]. When the thickness exceeds 4 u.c., which is the threshold for the conductivity at the interface [18], the interfacial property clearly shows that band bending of the CB edge brings the CB on the STO side below the Fermi level for 5-u.c. LAO grown on the TiO_2-terminated STO surface. According to the interfacial band diagram in Fig. 4(d), several critical points can be summarized. (1) The decay length of the charge carriers (λ) on the STO side is 0.8 nm for 5-u.c. LAO/STO [33]. The exponential decay of the carrier density distribution also suggests that more charge carriers are located within the decay length (λ) on the STO side of the interface, leading to the formation of two-dimensional electron gas. The observations from these experiments are consistent with the recently predicted decay length, which considers the electron-phonon interactions of the polar unit cells [34]. Scanning transmission electron microscopy of the charge redistribution in 5-u.c. LAO reveals similar results [35]. (2) The shift of the CB in the STO (ΔV) caused by band bending is approximately -0.31 eV for 5-u.c. LAO/STO. The magnitude of the band bending, including the band shift and the decay length λ, at the interface on the STO side also depends on the thickness of LAO films. The notched structure and the energy shift attributable to band bending in the STO layers in the interfacial region have been determined by *in situ* PES study in Ref. [16]. In the present STM work, the critical concerns regarding the electronic configurations at the LAO/STO interface, the spatial distribution of the electron gas, and the magnitude of the built-in electric field in LAO are demonstrated and discussed. (3) The band-gap shrinkage in STO near the interfacial LAO/STO region originated from the increasing carrier concentration at the interface. The local sheet carrier density can be estimated according to the confirmed thickness of the metallic region ($\lambda = 0.8$ nm) to be in the order of 10^{12} cm^{-2}–10^{13} cm^{-2} at the interface. This is consistent with the experimental results reported in Ref. [18]. (4) Data obtained by STM and STS directly display the electronic characteristic across the LAO/STO interface in the system. The magnitude of the built-in electric field across the 5-u.c. LAO is approximately 30 ± 5 meV/A. Since the polarity of atomic layers in LAO is along the [001] direction, the intrinsic built-in electric field should not be affected significantly owing to the STM measurements from the cross-sectional side, which approaches the interface perpendicularly. In addition, compared to the previous experimental work for this system [12], the influence of the surface boundary condition on the value of the built-in electric field in LAO from STM measurements is roughly 1/2 times that of the system. As the schematic band alignments of the 5-u.c. LAO/STO interfaces illustrated in Fig. 4(d), this picture outlines the spatial distribution, the charge density inside the STO, and the magnitude of the built-in electric field in LAO to atomic resolution.

In conclusion, STS techniques provide a definitive method to characterize the fascinating properties of complex oxide interfaces [36,37]. In this study, we demonstrate a unique approach to reveal the evolution of band alignments across LAO/STO heterostructures. The spatial distribution of the electron gas, the local carrier concentration of the metallic state in STO, and the magnitude of the built-in electric field in LAO are extracted. Direct evidence from

the STS of the band structure not only reveals the microscopic distribution of the charges but also demonstrates the band alignment across the polar LAO/STO interface.

The authors would like to thank the National Science Council of Taiwan, for financially supporting this research under Contracts No. NSC-101-2112-M-110 -007-MY2 and No. NSC-100-2119-M-009-003.

*Corresponding author.
ypchiu@mail.nsysu.edu.tw

[1] H. Takagi and H. Y. Hwang, Science **327**, 1601 (2010).
[2] A. Ohtomo and H. Y. Hwang, Nature (London) **427**, 423 (2004).
[3] M. Basletić, J.-L. Maurice, C. Carrétéro, G. Herranz, O. Copie, M. Bibes, É. Jacquet, K. Bouzehouane, S. Fusil, and A. Barthélémy, Nat. Mater. **7**, 621 (2008).
[4] J. Chakhalian, J. W. Freeland, H.-U. Habermeier, G. Cristiani, G. Khaliullin, M. van Veenendaal, and B. Keimer, Science **318**, 1114 (2007).
[5] J. Seidel *et al.*, Nat. Mater. **8**, 229 (2009).
[6] P. Yu *et al.*, Phys. Rev. Lett. **105**, 027201 (2010).
[7] Y. P. Chiu *et al.*, Adv. Mater. **23**, 1530 (2011).
[8] Y. Dong, R. M. Feenstra, R. Hey, and K. H. Ploog, J. Vac. Sci. Technol. B **20**, 1677 (2002).
[9] Y. Dong, R. M. Feenstra, M. P. Semtsiv, and W. T. Masselink, J. Appl. Phys. **103**, 073704 (2008).
[10] P. R. Willmott *et al.*, Phys. Rev. Lett. **99**, 155502 (2007).
[11] N. Nakagawa, H. Y. Hwang, and D. A. Muller, Nat. Mater. **5**, 204 (2006).
[12] G. Singh-Bhalla, C. Bell, J. Ravichandran, W. Siemons, Y. Hikita, S. Salahuddin, A. F. Hebard, H. Y. Hwang, and R. Ramesh, Nat. Phys. **7**, 80 (2011).
[13] R. Pentcheva and W. E. Pickett, Phys. Rev. Lett. **102**, 107602 (2009).
[14] G. Herranz *et al.*, Phys. Rev. Lett. **98**, 216803 (2007).
[15] A. Kalabukhov, R. Gunnarsson, J. Börjesson, E. Olsson, T. Claeson, and D. Winkler, Phys. Rev. B **75**, 121404(R) (2007).
[16] K. Yoshimatsu, R. Yasuhara, H. Kumigashira, and M. Oshima, Phys. Rev. Lett. **101**, 026802 (2008).
[17] K. Janicka, J. P. Velev, and E. Y. Tsymbal, Phys. Rev. Lett. **102**, 106803 (2009).
[18] S. Thiel, G. Hammerl, A. Schmehl, C. W. Schneider, and J. Mannhart, Science **313**, 1942 (2006).
[19] Several samples were tried, and consistent spectra on the STO surface away from the interface were also taken to be a reference to demonstrate the reproducibility.
[20] In conjunction with the theoretical modeling, we suggest that from our spectroscopic results, the cleaved surface of the LAO surface in the present work is the stable LaO-terminated surface.
[21] R. M. Feenstra, Phys. Rev. B **50**, 4561 (1994).
[22] R. M. Feenstra and J. A. Stroscio, J. Vac. Sci. Technol. B **5**, 923 (1987).
[23] The tip-induced accumulation of electrons in the states near the Fermi level could result in the tunneling currents at voltages corresponding to energies within the fundamental band gap of a semiconductor.
[24] Supporting materials addressing more discussions on the tip-induced band bending effect during STM measurements. See Supplemental Material at http://link.aps.org/supplemental/10.1103/PhysRevLett.109.246807 for the tip-induced band bending effect during STM measurements.
[25] G. J. De Raad, D. Bruls, P. Koenraad, and J. Wolter, Phys. Rev. B **66**, 195306 (2002).
[26] Y. P. Chiu, B. C. Huang, M. C. Shih, J. Y. Shen, P. Chang, C. S. Chang, M. L. Huang, M.-H. Tsai, M. Hong, and J. Kwo, Appl. Phys. Lett. **99**, 212101 (2011).
[27] N. Ishida, K. Sueoka, and R. M. Feenstra, Phys. Rev. B **80**, 075320 (2009).
[28] C. Park, Y. Seo, J. Jung, and D.-W. Kim, J. Appl. Physiol. **103**, 054106 (2008).
[29] J. Robertson and C. W. Chen, Appl. Phys. Lett. **74**, 1168 (1999).
[30] B. E. Park and H. Ishiwara, Appl. Phys. Lett. **82**, 1197 (2003); J. Krupka, R. G. Geyer, M. Kuhn, and J. H. Hinken, IEEE Trans. Microwave Theory Tech. **42**, 1886 (1994).
[31] X. Cai, C. D. Frisbie, and C. Leighton, Appl. Phys. Lett. **89**, 242915 (2006).
[32] Y. Li and J. Yu, J. Appl. Phys. **108**, 013701 (2010).
[33] R. Pentcheva and W. E. Pickett, J. Phys. Condens. Matter **22**, 043001 (2010).
[34] D. R. Hamann, D. A. Muller, and H. Y. Hwang, Phys. Rev. B **73**, 195403 (2006).
[35] A. Ohtomo, D. A. Muller, J. L. Grazul, and H. Y. Hwang, Nature (London) **419**, 378 (2002).
[36] N. P. Guisinger, T. S. Santos, J. R. Guest, T.-Y. Chien, A. Bhattacharya, J. W. Freeland, and M. Bode, ACS Nano **3**, 4132 (2009).
[37] T. Chien, J. Liu, J. Chakhalian, N. Guisinger, and J. Freeland, Phys. Rev. B **82**, 041101(R) (2010).